



Simple generic picture of tensile toughness in solid polymer blends

Debashish Mukherji ^{1,*}, Shubham Agarwal,² Tiago Espinosa de Oliveira,³ Céline Ruscher ² and Jörg Rottler^{1,4}

¹*Quantum Matter Institute, University of British Columbia, Vancouver BC V6T 1Z4, Canada*

²*Department of Mechanical Engineering, University of British Columbia, Vancouver BC V6T 1Z4, Canada*

³*Departamento de Farmacociências, Universidade Federal de Ciências da Saúde de Porto Alegre, Porto Alegre 90050-170, Brazil*

⁴*Department of Physics and Astronomy, University of British Columbia, Vancouver BC V6T 1Z1, Canada*



(Received 19 July 2022; revised 17 October 2023; accepted 19 October 2023; published 6 November 2023)

The tensile toughness \mathcal{T} of a brittle polymeric solid can be enhanced by blending a ductile polymer. While this common wisdom is generally valid, a generic picture is lacking that connects the microscopic details to the macroscopic nonlinear mechanics. Using all-atom and complementary generic simulations, we show how a delicate correlation between the side group contact density of the brittle polymers ρ_c and its dilution upon adding a second component controls \mathcal{T} . A set of chemically distinct systems follows a generic trend in \mathcal{T} with $d\rho_c/d\varepsilon$, where ε is the tensile strain. The observed trend is explained using a simple mechanical model based on the parallel spring analogy.

DOI: [10.1103/PhysRevMaterials.7.115601](https://doi.org/10.1103/PhysRevMaterials.7.115601)

I. INTRODUCTION

Polymers are widely used in designing light weight, high performance organic materials [1–4] that find use in items ranging from common household utensils to complex nanomaterials [1,5–8]. Because of their wide applicability, these materials are often exposed to a range of environmental conditions, such as temperature [9–12], pressure [10,13], and/or mechanical deformation [6,9,14–16]. Here, one important materials property is the ability to sustain large deformation [4,16–19].

Most known commodity polymers, such as poly(methyl methacrylate) (PMMA) [15,16], poly(lactic acid) (PLA) [4,16], and polystyrene (PS) [20], are brittle in their glassy states, i.e., small strain-to-fracture ε_f and low yield stress $\sigma_y \simeq 0.1$ GPa due to their weak van der Waals (vdW) monomer–monomer interactions, the strength of which is about $k_B T$ at the ambient temperature, where k_B is the Boltzmann constant [21]. On the other hand, σ_y of a polymer can be enhanced by about an order of magnitude when the monomer–monomer hydrogen bonds (H bond), having an interaction strength of about $4k_B T - 8k_B T$ [3], dominate materials properties, such as in poly(acrylamide) (PAM), poly(acrylic acid) (PAA), and poly(vinyl alcohol) (PVA). These H-bonded systems, however, can either be brittle or ductile depending on their respective (macro)molecular architectures. Given the above discussion, the mechanical response remains typically restricted in the single component polymeric systems and thus often limits their broad applications.

A common route to tune the tensile toughness $\mathcal{T} = \int_0^\infty \sigma(\varepsilon) d\varepsilon$ of a brittle organic solid is by blending in another polymer with relatively larger ductility and complementary component-wise interactions. Here, σ , $\varepsilon = \ln\{L(\varepsilon)/L_0\}$, $L(\varepsilon)$,

and L_0 are the true tensile stress and the true tensile strain, the instantaneous box length, and the initial box length, respectively. Experimentally relevant examples include, but are not limited to, PMMA-PLA [16,22], PAA-PVA blends [18], and/or PMMA-PVA [23]. These systems remain fairly miscible over the full range of mixing concentrations x_1 .

In general, \mathcal{T} of a blend varies monotonically between the two pure phases with x_1 [18]. On the contrary, a set of recent experiments on PMMA-PLA blends have reported a nonmonotonic variation in \mathcal{T} with concentration [16]. This behavior was attributed to the formation of “so-called” co-continuous phases, with an estimated length scale of about several μm [16,22]. Here, a set of midsized all-atom simulations have found a similar trend in \mathcal{T} [24], suggesting that the formation of the co-continuous phase may not be a necessary criterion for the enhancement of \mathcal{T} in polymers.

Traditionally, extensive research has been conducted to understand the mechanics of polymeric materials, both from the experimental [4,16,18,20] and the simulation [14,15,17,24] communities. Here, however, most simulation studies usually deal with single component systems and also predominantly at the (mesoscopic) generic level, where all-atom details are drastically coarse-grained [21]. While such models are extremely useful in dealing with generic polymer properties, they often (in their pristine form) lack the details that play a key role in materials properties, unless the generic model is specifically tuned to reproduce certain properties of interest. In particular, when dealing with polymer blends having very specific macromolecular structures and interactions [16,18,24], special attention should be paid. Therefore, a better understanding of the monomer-level interactions is needed to achieve a predictive mechanical response of the polymer blends, which to the best of our knowledge is lacking.

In this work, we investigate the commodity organic solids with the goals to (1) understand the effect of blending on

*debashish.mukherji@ubc.ca

the mechanical response of brittle systems, (2) show how the monomeric structures play a key role in dictating the materials properties, (3) connect the microscopic interaction details to the macroscopic nonlinear mechanics, and (4) propose how the behavior of many different chemically specific polymeric materials can be understood within one generic framework. To achieve the above goals, we combine all-atom and complementary generic molecular-dynamics simulations with a simple mechanical model.

The remainder of this work is organized as follows: In Sec. II we describe the model and method related details. The results are discussed in Sec. III and, finally, the conclusions are drawn in Sec. IV.

II. MODEL AND METHOD

A. All-atom model

For the all-atom simulations, we have chosen experimentally relevant vdW and H-bonded commodity polymers (i.e., PMMA, PAM, PAA, PLA, and PVA) and polymer blends (i.e., PMMA-PVA, PAA-PVA, and PMMA-PLA). These three blends are chosen because their microscopic interactions are the combinations of vdW and H-bonded polymers (PMMA-PVA), both H-bonded polymers (PAA-PVA), and both vdW polymers (PMMA-PLA) and thus covering two common commodity polymer interactions. Note that we have performed the simulations for all systems in this work, aside from the PMMA-PLA trajectories that were obtained earlier [24] and reanalyzed here. The monomer mole fractions are varied between $0.0 \leq x_i \leq 1.0$ in steps of 0.25. In this study, $x_i = 0.0$ always corresponds to the pure phase of brittle polymer (BP) and the pure second polymer (SP) at $x_i = 1.0$. The OPLS-AA parameters are used for PAA, PLA, and PVA [25], while the modified atomic partial charges are used for PAM [26] and PMMA [27]. The chain length $N_\ell = 30$ monomers is chosen for all systems except PAM, where $N_\ell = 32$. The simulations are performed using the GROMACS molecular-dynamics package [28]. More system specific details are shown in the Supplemental Material Sec. S1A [29].

B. Generic model

The bead-spring polymer model is used for the generic simulations [21]. Note that the default bead-spring model is highly ductile [14]. Therefore, inspired by the all-atom BP architectures, we have parametrized a brush-like polymer with one short (stiff) dimer attached to every second backbone monomer, blended with the (ductile) linear chains. The generic monomer-monomer interactions are tuned to weakly mimic the atomistic PMMA-PLA blends. The backbone chain length is taken as $N_\ell = 30$. The generic simulations are performed using the LAMMPS package [30]. A detailed discussion of the generic model is presented in the Supplemental Material Sec. S1B [29]. The numbers representative of the hydrocarbons are the units of length $d = 0.5$ nm, energy $\epsilon = 30$ meV, time $t_o = 3$ ps, and pressure $p_o = 40$ MPa [21]. Note that, for simplicity of presentation, we have converted all generic units into the real units using the above estimates.

III. RESULTS AND DISCUSSIONS

In Figs. 1(a)–1(c) we show the stress-strain behavior of three different atomistic blends under uniaxial tensile deformation. As expected, blending (ductile) SPs drive (brittle) BPs to enhanced ductility. Ideally one can argue, if SPs have their glass transition temperatures T_g much smaller than BP (and thus remain in their rubbery phases), the ductility or \mathcal{T} may increase via rubber plasticity. In our case, however, all polymers have $T_g \simeq 355$ – 390 K (as measured in the experiments) [16,31], while the simulation results have reported $T_g \simeq 400$ K [24,32]. Because our simulations are performed at $T = 300$ K, the individual components of a blend remain deep in their respective glassy states [31,32]. This readily excludes any explanation purely based on T_g and thus a better understand of mechanics is needed in the multicomponent polymers.

A. Molecular-level interlocking and its connection to the stress-strain behavior

A comparative analysis of the monomer structures of BP and SP reveals that one major difference between these two sets is the presence of bulky side groups in BPs (see PAA and PMMA structures in the insets of Fig. 1), while SPs are relatively smooth (see PVA and PLA structures in the insets of Fig. 1). Here, it is known that the side groups of BPs are rather stiff and thus form extremely rugged (instantaneous) structural corrugation along the chain contours. Corrugation (or more generally speaking, the breaking of translational Galilean invariance) is a necessary “ingredient” to exert the shear forces upon deformation. Note also that the side groups can flip-flop normal to the chain contours in the melts, while these structural fluctuations are relatively frozen in their glassy states. In this context, it has been previously shown that the presence of stiff side chains may serve as a necessary criterion to control the brittleness in a solid PMMA [15].

Within the picture discussed above, the side groups of two or more neighboring chains can interlock [33], shown by the schematic in Fig. 2(a). Here, the side groups can interact by either vdW or H bonds. The stronger the side chain interaction, the larger the σ_y values. We find $\sigma_y^{\text{PMMA}} < \sigma_y^{\text{PAA}} < \sigma_y^{\text{PAM}}$, see the Supplemental Material Fig. S9 [29]. This is expected because two PMMA side chains interact via weak vdW interaction, while two PAA and two PAM can form 0.84 and 1.52 H bonds per monomer, respectively. When a pure BP is deformed, the rigid side chain contacts break via relative motion of the chains and thus the sliding molecules overcome the effective free-energy barriers. Such broken contacts initiate cavitation at around the yield strain, i.e., $\epsilon_y \simeq 0.1$ – 0.2 , see Fig. 1. Beyond ϵ_y , the systems go into the flow regime with growing voids, leading to their coalescence and ultimate fracture.

When the SP molecules are added, they lubricate the side chain contacts and thus dilute their density ρ_c , see the schematic in Fig. 2(b). This microscopic molecular arrangement increases ϵ_f and also hinders the growing voids via rearrangements of SPs. The extent of molecular ruggedness that a molecule feels, while moving in the homogeneous bulk,

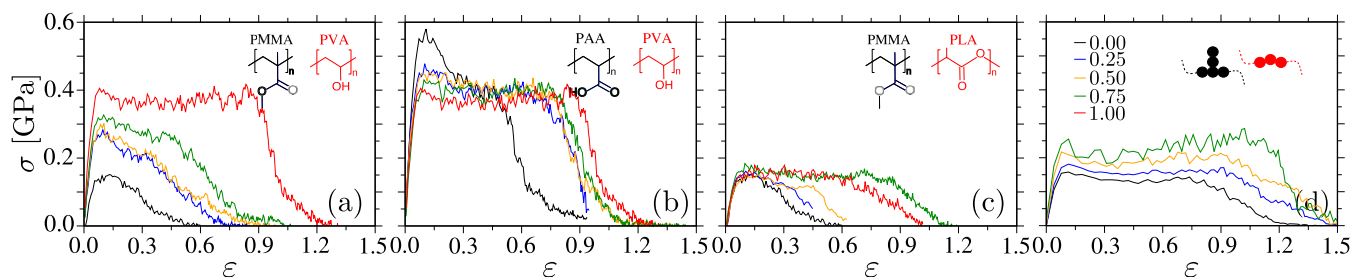


FIG. 1. True stress σ as a function of true strain ϵ for three different atomistic blends, namely, (a) poly(methyl methacrylate) (PMMA) and poly(venyl alcohol) (PVA), (b) poly(acrylic acid) (PAA) and PVA, (c) PMMA and poly(lactic acid) (PLA), and (d) the generic model. The data are shown for five different PVA and PLA and four (generic) linear chain monomer mole fractions x_i . Here, $x_i = 0.0$ corresponds to the pure brittle phase. The corresponding monomer structures are shown in the insets. σ for the generic model is converted using a factor $p_o = 40$ MPa [21]. Note that the data for PMMA-PLA blends are taken from Ref. [24].

is related to x_i and has a direct implication on a moving polymer. The mean-squared-displacement $C(t)$ data, shown in the Supplemental Material Figs. S2 and S3 [29], provide evidence that the polymer diffusion D increases with increasing x_i . Within the linear response, different damping contributions are linearly additive and thus the effective damping $\gamma \propto 1/D$. Furthermore, following $C(t)$ in the Supplemental Material Figs. S2 and S3 [29], it becomes apparent that the molecular-level ruggedness (or corrugation) reduces with increasing x_i . In the glassy state, we also expect the relative ruggedness across different samples to remain the same. Note that the statement above does not aim to make a direct quantitative comparison between the melt and the glassy states, rather only a qualitative comparison without attempting to discuss the time-temperature superposition.

The systems investigated in this study have larger ductility than the experimentally reported values [4,16,18,20]. This is particularly because the quenching rates (i.e., from melt to glass) in the simulations are usually several orders of magnitude faster than the corresponding experiments and thus lead (in most cases) to poorer annealed samples [34]. Such samples usually have a broad distribution of σ , leading to a

larger ϵ_f and also in some cases rather long decaying tails in the stress-strain curves, see Figs. 1(a)–1(c). On the contrary, the well-annealed samples have a narrow distribution in σ and thus all sites fail almost at once, as evident from the smaller ϵ_f . Here, however, it is important to note that our simulation samples are prepared using an identical protocol and, considering that this study aims at the relative trends and not exact numbers, we believe Fig. 1 presents a reasonable picture.

If the observation discussed above is generic, the trends in Figs. 1(a)–1(c) should also be visible in a generic (chemically independent) model, only by incorporating the molecular ruggedness. In Fig. 1(d) the generic data are presented. It can be appreciated that the trends observed in Figs. 1(a)–1(c) is also reproduced by the generic model. When the side groups of BP are made flexible (i.e., preventing them to interlock), the same generic systems can become significantly tougher, see the Supplemental Material Fig. S10 [29].

B. Interlocking contact density and tensile toughness

So far we have only presented a qualitative picture of mechanics in blends. We now attempt to draw a more quantitative comparisons between $\rho_c(\epsilon)$ and \mathcal{T} . Here, $\rho_c(\epsilon) = N_c(\epsilon)/v(\epsilon)$, with $N_c(\epsilon)$ and $v(\epsilon)$ being the number of side chain contacts and the instantaneous system volume, respectively. In the all-atom simulations, $N_c(\epsilon)$ is calculated when the center of masses of two neighboring side chains are within a distance $r_{\min} \leq 0.65$ nm, i.e., the minima after the first peak of pair distribution function. In the generic model, $r_{\min} \leq 1.5 \sigma$ [35].

In Fig. 3 we show $\rho_c(\epsilon)$ for the all-atom and the generic systems. It can be appreciated that (a) $\rho_c(\epsilon)$ decreases with increasing ϵ , which is expected because tensile deformation breaks the side chain contacts. (b) Increasing x_i generally dilutes $\rho_c(\epsilon)$, hence the weaker decay rates are observed for $\epsilon > \epsilon_y$ (shown by the vertical dashed lines in Fig. 3).

The individual data sets in Fig. 3 show two different $d\rho_c(\epsilon)/d\epsilon$ regions. A relatively rapid initial decay for $\epsilon_y < 0.2$ (in all-atom) and $\epsilon_y < 0.1$ (in generic), where $d\rho_c(\epsilon)/d\epsilon$ is dominated by the disruption between side groups, see Fig. 1. The second linear decay beyond ϵ_y occurs when the individual systems reach the stationary flow regime (or the plastic flow), where the voids grow by breaking the side chain contacts to control \mathcal{T} and also SPs rearrange to control the void growth.

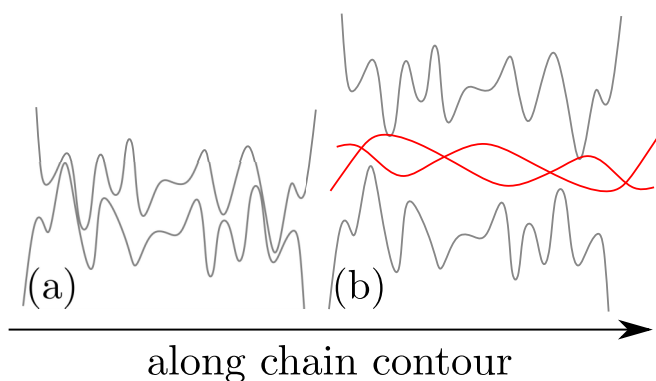


FIG. 2. Schematic representations of the direct contacts between (a) the brittle polymers (BP) before and (b) after including the second polymer (SP). For the simplicity of presentation, the one-dimensional projection of the effective roughness (or the effective free-energy landscape) of the molecules along the chain contours is shown. The gray and red lines represent (rugged) BP and (smooth) SP molecules, respectively.

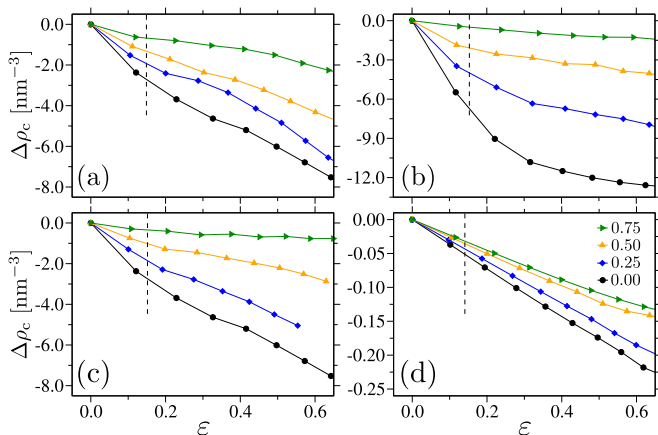


FIG. 3. Density of side chain contacts $\Delta\rho_c = \rho_c(\varepsilon) - \rho_c(0)$ as a function of true strain ε between the neighboring monomers of the brittle polymers in the blends of (a) poly(methyl methacrylate) (PMMA) and poly(vinyl alcohol) (PVA), (b) poly(acrylic acid) (PAA) and PVA, (c) PMMA and poly(lactic acid) (PLA), and (d) the generic model. For better visibility of the relative variation in the data, we have shifted all curves with respect to $\rho_c(0)$ of the unstrained system, i.e., at $\varepsilon = 0$. In the generic model, $d\rho_c/d\varepsilon$ is scaled using the unit conversion $d = 0.5$ nm [21]. Data for PLA-PMMA blends is derived from our earlier simulation trajectories in Ref. [24]. The vertical dashed lines show the ε values at the yield points, see Fig. 1.

We calculate the slopes $S = d\rho_c(\varepsilon)/d\varepsilon$ in the stationary flow regimes, where the behavior is reasonably well described by a simple linear form $\rho_c(\varepsilon) = \rho_c + S\varepsilon$.

Figure 4 shows the variation of toughness-to-strength ratio \mathcal{T}/σ_y with $S\ell_o^3$. Here, ℓ_o is a microscopic length scale equal to the equilibrium distance between the center of masses of

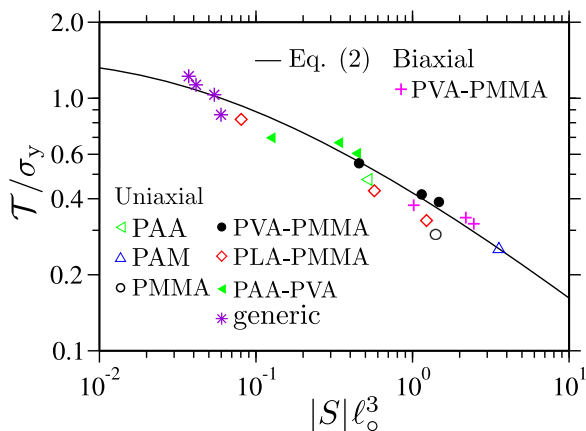


FIG. 4. A master curve relating the normalized tensile toughness \mathcal{T}/σ_y with the change in side chain contact density ρ_c upon deformation, as quantified by the slope $S = d\rho_c(\varepsilon)/d\varepsilon$. Here, σ_y and ℓ_o are the yield stress and the equilibrium distance between the center of masses of two side groups of the brittle polymers, respectively. Note also that S is negative by definition and thus we only use its magnitude $|S|$. The line is a fit to the data using Eq. (3). While most data sets are shown for uniaxially deformed samples, we also present one case study in which a set of PMMA-PVA blends is biaxially deformed.

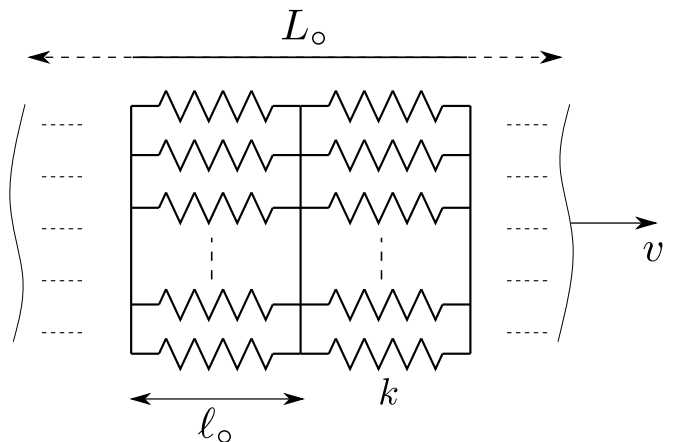


FIG. 5. A schematic representation of the parallel spring model developed in this study. Here, a solid polymer blend is considered as a three-dimensional network of springs. Within a simple approximation, a system consists of N_s slices of parallel springs, each containing on average n_c springs, along the direction of deformation with velocity v . L_o and ℓ_o are the unstrained box length and equilibrium spring length, respectively. k is the spring constant.

two side groups of BP, which ranges between 0.45–0.55 nm for the all-atom systems. For the generic, we have chosen $\ell_o = 2^{1/6}d \simeq 0.56$ nm, i.e., the distance between the particles of the side groups. Note that ℓ_o values are estimated from the positions of first correlation peaks in their pair distribution functions. It can be appreciated that our choice of chemical specific systems and the generic system fall onto one empirical master curve. Here, most data sets are obtained under uniaxial loading, where mechanics is dominated by the shear forces of sliding molecules. One set of data under biaxial loading, where the cavitation is enhanced (see the Supplemental Material Figs. S6 and S7 [29]), also supports the same empirical trend.

C. A simple model based on the parallel spring analogy

The data sets in Fig. 4 show a reasonable correlation across several samples; it is, however, also important to investigate if this behavior can be explained within a description by only incorporating some microscopic details. For this purpose, we use a simple (mechanical) model based on the parallel springs analogy (PSA) [36]. PSA has a rather broad application ranging across linear vibration theory [37], polymeric materials [38], random fiber networks [39], and mechanics of a single fiber [40].

In this simple model, an organic solid is modeled as a network of three-dimensional springs consisting of N_s slices along the direction of deformation, where each such slice on average consists of n_c parallel springs with stiffness k_i , see Fig. 5. Here, one side chain interlocking represents one spring contact. If we consider that all contacts contribute equally to the loading, i.e., $k_i \simeq k$, the force within one slice reads $f(\delta) = \sum_{i=1}^{n_c} k_i \delta = kn_c(\delta)\delta$ and thus the total force on a sample will also be $F(\delta) = kn_c(\delta)\delta$, which stems from the fact that the slices are connected in series (i.e., similar to the springs in series approximation) and thus the total force is the same as the force within a slab [41]. Under

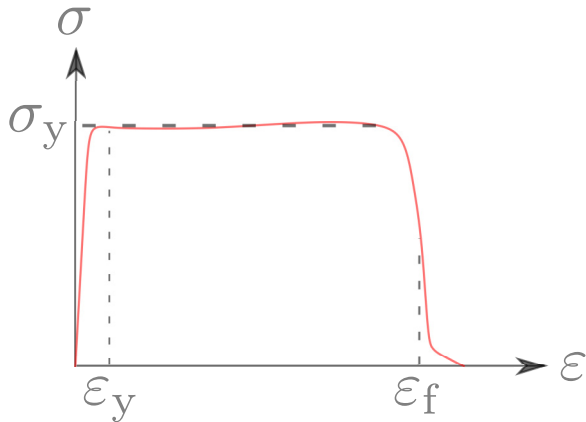


FIG. 6. A schematic representation of the stress-strain behavior with a well-defined rectangular ductile region. Here, ε_y and ε_f are the yield and failure strains, respectively.

the affine assumption, the local (microscopic) displacement $\delta = \ell_o(e^\varepsilon - 1)$, where $\varepsilon = \ln\{\ell(\varepsilon)/\ell_o\}$ is the true strain. Here ℓ_o is the equilibrium distance between the centers of mass of two side groups of BP. The tensile stress σ then follows from F using

$$\sigma(\varepsilon) = k \frac{n_c(\varepsilon)\varepsilon\ell_o}{A(\varepsilon)} = k\rho_c(\varepsilon)\varepsilon\ell_o\ell(\varepsilon), \quad (1)$$

where $\rho_c(\varepsilon) = N_s n_c(\varepsilon)/v(\varepsilon)$. $A(\varepsilon)$, $v(\varepsilon) = A(\varepsilon)L(\varepsilon)$, and $\ell(\varepsilon) = \ell_o e^\varepsilon$ are the instantaneous cross-sectional area in the lateral directions, the instantaneous volume, and the slice length along the direction of deformation, respectively. $L(\varepsilon) = N_s \ell(\varepsilon)$ is the total instantaneous length of a system. Following this argument, we can now write the toughness-to-strength ratio as

$$\frac{\mathcal{T}}{\sigma_y} = \frac{1}{\sigma_y} \int_0^{\varepsilon_f} \sigma(\varepsilon) d\varepsilon = \frac{k\ell_o^2}{\sigma_y} \int_0^{\varepsilon_f} \rho_c(\varepsilon) e^\varepsilon (e^\varepsilon - 1) d\varepsilon. \quad (2)$$

Equation (2) leads to an empirical solution,

$$S\ell_o^3 \simeq \frac{1 - \frac{k'\ell_o^3\rho_o}{\sigma_y} \sum_{i=1}^4 b_i \left(\frac{\mathcal{T}}{\sigma_y}\right)^i}{\frac{k'}{\sigma_y} \sum_{i=1}^4 c_i \left(\frac{\mathcal{T}}{\sigma_y}\right)^{i+1}}, \quad (3)$$

where $k' = k/\ell_o$ is a modulus and the constant prefactors b_i and c_i are in listed in Ref. [42]. Going from Eq. (2) to Eq. (3), we enforce a condition that $d\sigma/d\varepsilon = 0$ for $\varepsilon > \varepsilon_y$ and thus one can approximate $\varepsilon_f \simeq \mathcal{T}/\sigma_y$, see the schematic in Fig. 6.

Equation (3) is plotted as a solid line in Fig. 4, with $k'\ell_o^3\rho_o/\sigma_y < 1$. It can be appreciated that the model prediction of Eq. (3) agrees reasonable well with the simulation data in Fig. 4. This further reinforces a picture directing at a possible route towards the tunability in \mathcal{T}/σ_y and its links to the atomic-level details. Note that, even when the model prediction of Eq. (3) uses a fixed k (i.e., linear), the model itself is nonlinear due to the behavior of ρ_c .

We note in passing that Eq. (3) is derived for the true strain estimates. However, for the relatively smaller ε values (as in our cases), the model prediction is dominated by the leading-order terms (i.e., for $i > 2$), while the higher-order terms only contribute less than 5% to the data shown in Fig. 4.

With the model presented in this study, we do not wish to claim that our treatment captures all the necessary ingredients of the underlying complex macromolecular systems. Instead, we have attempted to propose a simple model that can reasonably capture the functional dependence shown in Fig. 4. Of course, one may formulate a model that incorporates more system-specific complexities that (a) will be extremely nontrivial given that there are many competing interactions in these systems. (b) Our simple model captures most of the important features within the leading-order contributions, while the other complexities are expected to play only minor roles.

IV. CONCLUSION

We have performed large-scale molecular-dynamics simulations to study the mechanics of solid commodity polymer blends. We show how a delicate balance between the (macromolecular) side chain organizations, resultant corrugation along the chain contour, and their interlocking controls the tensile toughness \mathcal{T} of a polymeric material. Our study establishes a relationship between the microscopic interactions and the macroscopic nonlinear mechanics, which follows a universal empirical relationship across a wide range of polymeric systems. To better understand this behavior, we have also formulated a simple model based on the *springs in parallel* analogy. The simplified picture presented here may serve as a guiding tool for the development of advanced functional materials with tunable and predictive mechanical properties.

It will certainly require more detailed experiments to validate our scenario. One plausible path might be to follow the protocol presented in an earlier study of one of us [43], where a proton nuclear magnetic resonance (NMR) setup was used to obtain the local side chain organizations between the neighboring nonbonded monomers. Here, we expect that the on-the-fly NMR measurements (at different ε) might give direct information about ρ_c and thus can lead to a better understanding of the underlying atomistic picture in these commodity organic solids.

ACKNOWLEDGMENTS

D.M. thanks C. Marques, K. Kremer, and T. Laschütza for stimulating discussions. This research was undertaken thanks, in part, through the Canada First Research Excellence Fund (CFREF), Quantum Materials and Future Technologies Program. D.M. further thanks the ARC Sockeye facility of University of British Columbia where the simulations are performed.

D.M. proposed, designed, and conceptualized this study, parametrized the generic model, ran the simulations, proposed the interlocking picture, and wrote the draft. S.A. formulated the parallel spring model. T.E.O. prepared the GROMACS simulation setups and ran some initial simulations. C.R. provided the LAMMPS input scripts. J.R. suggested Ref. [16] and co-proposed this study. D.M. and J.R. co-analyzed Fig. 4 and co-wrote the reply to the referees.

- [1] M. A. Cohen-Stuart, W. T. S. Huck, J. Genzer, M. Müller, C. Ober, M. Stamm, G. B. Sukhorukov, I. Szleifer, V. V. Tsukruk, M. Urban, F. Winnik, S. Zauscher, I. Luzinov, and S. Minko, *Nat. Mater.* **9**, 101 (2010).
- [2] M. Müller, *Prog. Polym. Sci.* **101**, 101198 (2020).
- [3] D. Mukherji, C. M. Marques, and K. Kremer, *Annu. Rev. Condens. Matter Phys.* **11**, 271 (2020).
- [4] X. Zhao, H. Hu, X. Wang, X. Yu, W. Zhou, and S. Peng, *RSC Adv.* **10**, 13316 (2020).
- [5] W. Shi, Z. Shuai, and D. Wang, *Adv. Funct. Mater.* **27**, 1702847 (2017).
- [6] K. S. Toohey, N. R. Sottos, J. A. Lewis, J. S. Moore, and S. R. White, *Nat. Mater.* **6**, 581 (2007).
- [7] M. Sharifi, C. W. Jang, C. F. Abrams, and G. R. Palmese, *J. Mater. Chem. A* **2**, 16071 (2014).
- [8] D. Mukherji and K. Kremer, *Polymers (Basel, Switz.)* **15**, 3229 (2023).
- [9] R. S. Hoy and M. O. Robbins, *J. Polym. Sci., Part B: Polym. Phys.* **44**, 3487 (2006).
- [10] V. A. Harmandaris, J. Floudas, and K. Kremer, *Macromolecules (Washington, DC, U. S.)* **44**, 393 (2011).
- [11] W. Liu and W. Zhai, *J. Res. Updates Polym. Sci.* **4**, 139 (2015).
- [12] J. Wu and D. Mukherji, *Comput. Mater. Sci.* **211**, 111539 (2022).
- [13] W.-P. Hsieh, M. D. Losego, P. V. Braun, S. Shenogin, P. Koblinski, and D. G. Cahill, *Phys. Rev. B* **83**, 174205 (2011).
- [14] J. Rottler and M. O. Robbins, *Phys. Rev. E* **68**, 011507 (2003).
- [15] K. Fujimoto, Z. Tang, W. Shinoda, and S. Okazaki, *Polymer* **178**, 121570 (2019).
- [16] X. Hou, S. Chen, J. J. Koh, J. Kong, Y.-W. Zhang, J. C. C. Yeo, H. Chen, and C. He, *ACS Macro Lett.* **10**, 406 (2021).
- [17] T. W. Rosch, J. K. Brennan, S. Izvekov, and J. W. Andzelm, *Phys. Rev. E* **87**, 042606 (2013).
- [18] Q. Huang, C. Wan, M. Loveridge, and R. Bhagat, *ACS Appl. Energy Mater.* **1**, 6890 (2018).
- [19] M. Huang and C. F. Abrams, *Macromol. Theory Simul.* **28**, 1900030 (2019).
- [20] P. Antich, A. Vázquez, I. Mondragon, and C. Bernal, *Composites, Part A* **37**, 139 (2006).
- [21] K. Kremer and G. S. Grest, *J. Chem. Phys.* **92**, 5057 (1990).
- [22] K. Le, R. Lehman, J. Remmert, K. Vanness, P. M. L. Ward, and J. D. Idol, *J. Biomater. Sci., Polym. Ed.* **17**, 121 (2006).
- [23] A. M. Kadim, A. D. Abdulkareem, A. J. K. Alrubaie, and K. H. Abass, *Mater. Today: Proc.* **80**, 2474 (2023).
- [24] D. Mukherji, T. E. de Oliveira, C. Ruscher, and J. Rottler, *Phys. Rev. Mater.* **6**, 025606 (2022).
- [25] W. L. Jorgensen, D. S. Maxwell, and J. Tirado-Rives, *J. Am. Chem. Soc.* **118**, 11225 (1996).
- [26] T. E. de Oliveira, D. Mukherji, K. Kremer, and P. A. Netz, *J. Chem. Phys.* **146**, 034904 (2017).
- [27] D. Mukherji, C. M. Marques, T. Stühn, and K. Kremer, *Nat. Commun.* **8**, 1374 (2017).
- [28] S. Pronk, S. Páll, R. Schulz, P. Larsson, P. Bjelkmar, R. Apostolov, M. R. Shirts, J. C. Smith, P. M. Kasson, D. van der Spoel, B. Hess, and E. Lindahl, *Bioinformatics* **29**, 845 (2013).
- [29] See Supplemental Material at <http://link.aps.org/supplemental/10.1103/PhysRevMaterials.7.115601> for the model related details; system equilibration and morphology; tensile toughness calculations; and system size effects, which also includes Refs. [44–49].
- [30] S. Plimpton, *J. Comput. Phys.* **117**, 1 (1995).
- [31] J. Brandrup, E. H. Immergut, and E. A. Grulke, *Polymer Handbook*, 2 Volumes Set (Wiley, New York, 2003), 4th ed.
- [32] C. Ruscher, J. Rottler, C. E. Boott, M. J. MacLachlan, and D. Mukherji, *Phys. Rev. Mater.* **3**, 125604 (2019).
- [33] Our study deals with a set of rather short chain lengths and thus there is a low probability of a chain to fold onto itself, where the most dominant contribution to interlocking comes from the neighboring chains and not within a chain.
- [34] Quenching rates in simulations are usually significantly higher than the experiments due to the obvious computational limitations, especially when dealing with the all-atom trajectories of reasonably big system sizes. Of course, one can use particle swapping protocols to better anneal a system, which is, however, beyond the scope of our work.
- [35] D. Mukherji and C. F. Abrams, *Phys. Rev. E* **79**, 061802 (2009).
- [36] K. Symon, *Mechanics* (Addison-Wesley, UK, 1971).
- [37] J. B. Vernon, *Linear Vibration Theory* (John Wiley and Sons, New York, 1967).
- [38] J. D. Ferry, *Viscoelastic Properties of Polymers*, 3rd ed. (Wiley & Sons, New York, 1980).
- [39] R. C. Picu, *Soft Matter* **7**, 6768 (2011).
- [40] F. Meng and E. M. Terentjev, *Polymers (Basel, Switz.)* **9**, 52 (2017).
- [41] Within our simple model, different slices form an effective springs-in-series-like arrangement. Therefore, under the affine deformation, the total force in a system is the same as the force within a slab.
- [42] $b_1 = b_2 = 1/2$, $b_3 = b_1/2$, $b_4 = b_1/10$, $c_1 = 1/3$, $c_2 = 3/8$, $c_3 = 1/5$, and $c_4 = 1/24$.
- [43] D. Mukherji, M. Wagner, M. D. Watson, S. Winzen, T. E. de Oliveira, C. M. Marques, and K. Kremer, *Soft Matter* **12**, 7995 (2016).
- [44] H. J. C. Berendsen, J. P. M. Postma, W. F. van Gunsteren, A. DiNola, and J. R. Haak, *J. Chem. Phys.* **81**, 3684 (1984).
- [45] L. Pigard, D. Mukherji, J. Rottler, and M. Müller, *Macromolecules (Washington, DC, U. S.)* **54**, 10969 (2021).
- [46] G. Bussi, D. Donadio, and M. Parrinello, *J. Chem. Phys.* **126**, 014101 (2007).
- [47] M. Doi and S. F. Edwards, *The Theory of Polymer Dynamics* (Oxford Science Publications, UK, 1986).
- [48] C. M. Hansen, *Hansen Solubility Parameters, A User's Handbook* (CRC Press, Boca Raton, 2000).
- [49] C. Chen, M. K. Singh, K. Wunderlich, S. Harvey, C. J. Whitfield, Z. Zhou, M. Wagner, K. Landfester, I. Lieberwirth, G. Fytas, K. Kremer, D. Mukherji, D. Y. W. Ng, and T. Weil, *Nat. Commun.* **12**, 3959 (2021).